New Phytologist

Research

C_4 maize and sorghum are more sensitive to rapid dehydration than C_3 wheat and sunflower

Chandra Bellasio[1,2,3], Hilary Stuart-Williams[3], Graham D. Farquhar[3] and Jaume Flexas[2]

[1]Laboratory of Theoretical and Applied Crop Ecophysiology, School of Biology and Environmental Science, University College Dublin, Belfield, Dublin 4, Ireland; [2]Biology of Plants Under Mediterranean Conditions, Department of Biology, University of the Balearic Islands, Illes Balears, Palma, 07122, Spain; [3]Research School of Biology, Australian National University, Acton, ACT, 2601, Australia

Author for correspondence:
Chandra Bellasio
Email: chandra.bellasio@ucd.ie

Received: *10 July 2023*
Accepted: *3 September 2023*

New Phytologist (2023)
doi: 10.1111/nph.19299

Key words: dehydration, drought, nonstomatal limitation, photosynthesis, stress, turgor.

Summary

- The high productive potential, heat resilience, and greater water use efficiency of C_4 over C_3 plants attract considerable interest in the face of global warming and increasing population, but C_4 plants are often sensitive to dehydration, questioning the feasibility of their wider adoption.
- To resolve the primary effect of dehydration from slower from secondary leaf responses originating within leaves to combat stress, we conducted an innovative dehydration experiment. Four crops grown in hydroponics were forced to a rapid yet controlled decrease in leaf water potential by progressively raising roots of out of the solution while measuring leaf gas exchange.
- We show that, under rapid dehydration, assimilation decreased more steeply in C_4 maize and sorghum than in C_3 wheat and sunflower. This reduction was due to a rise of nonstomatal limitation at triple the rate in maize and sorghum than in wheat and sunflower.
- Rapid reductions in assimilation were previously measured in numerous C_4 species across both laboratory and natural conditions. Hence, we deduce that high sensitivity to rapid dehydration might stem from the disturbance of an intrinsic aspect of C_4 bicellular photosynthesis. We posit that an obstruction to metabolite transport between mesophyll and bundle sheath cells could be the cause.

Introduction

Drought is a major factor that limits crop growth and productivity. It is estimated that drought affects > 75% of major global crops such as maize, rice, soy, and wheat leading to economic losses of *c.* €166 billion annually (naro.go.jp). While many studies have focussed on the impact of drought on crop yield, less attention has been given to photosynthetic responses that occur in crops during drought stress. When plants are subject to water shortage, they show complex responses, ultimately depressing net CO_2 assimilation (A). The difference in assimilation relative to the initial value is called water limitation (L_W). Stomata, the gateways of gas exchange through leaves, generally respond rapidly to environmental changes. The reduction in stomatal conductance (g_S) saves water, but hinders CO_2 intake, consequently increasing a component of L_W termed stomatal limitation (L_S). The other residual components of water limitation are collectively referred to as nonstomatal limitation (L_{NS}; where $L_W = L_S + L_{NS}$) grouping the effect of all mechanisms other than stomatal closure. These mechanisms include reductions in biochemical activities and in the efficiency of energy conversion processes, as well as structural changes in the plant's anatomy that can affect intercellular and intracellular CO_2 and bicarbonate diffusion, light interception, water transport and nutrient uptake, source–sink dynamics, *etc.* (Lawlor, 2002; Lawlor & Cornic, 2002).

Our most productive crops and biofuel producers, such as maize, sorghum, sugar cane, and *Miscanthus* use C_4 photosynthesis. C_4 plants evolved a variant of the ancestral C_3 photosynthetic pathway that confers potentially high rates of assimilation under high temperatures and light intensities, when C_3 plants falter (Bellasio & Farquhar, 2019). This has recently been attracting a resurgent wave of interest in the face of global warming and population growth (Furbank, 2016). In essence, C_4 photosynthesis is a biochemical carbon concentrating mechanism (CCM) operating in addition to the C_3 pathway of assimilation. The CCM pumps CO_2 from the atmosphere to deep inside the leaf, through an ATP-dependent cycle of carboxylation in the mesophyll (M), and decarboxylation in a partially isolated compartment, the bundle sheath (BS) through numerous plasmodesmata (Danila *et al.*, 2018). CO_2 concentration is therefore high close to Rubisco, thereby minimising energy-costly photorespiration (Bellasio *et al.*, 2014).

C_4 plants are highly responsive to water shortage (Ghannoum, 2009). For instance, in a phylogenetically controlled experiment on grasses, Taylor *et al.* (2010) showed that assimilation decreased on average 41% in C_4 and 32% in C_3 species over 5 wk. While in C_3 plants, stomatal limitation is substantial,

thanks to the CCM C_4 plants can generally maintain a steep stomatal concentration gradient of CO_2, thus suffering little stomatal limitation, and L_W mainly comprises L_{NS} (Bellasio *et al.*, 2018). Ripley *et al.* (2010) found that L_{NS} accounted for 50% of the decline in A with declining soil moisture for C_4 grass species, compared with 25% for closely related C_3 species, and that the predominance of L_{NS} slowed the recovery of C_4 photosynthesis following subsequent increases in soil moisture. Although it is known that L_{NS} appears much faster in C_4 than in C_3 plants (Ghannoum *et al.*, 2003; Ripley *et al.*, 2007; Ghannoum, 2009), it has to be mentioned that most previous studies analysed medium-term imposition of water stress, over the course of days to a few weeks. This can mask the direct effects of the stress itself ('strain') with the plant's own responses to combat the stress ('tolerance' mechanisms). Additionally, in the literature, the response is often related to the timing of treatment imposition rather than the intensity of the stress, which is what plants sense, and which is often measured by water potential. The comparison between C_3 and C_4 plants is complicated by the fact that C_4 plants often operate at lower g_S, and this saves water resulting in less negative water potential for C_4 than C_3 plants, for example Taylor *et al.* (2014) and Quirk *et al.* (2019b).

The responses of stomata and L_{NS} to water deficit are critical components of leaf and canopy models (Yang *et al.*, 2019), which describe the growth, evolution, and current distribution of C_3 and C_4 plants (Zhou *et al.*, 2018). While there are multiple stomatal models available, including C_3 and C_4 empirical models (Collatz *et al.*, 1992; Damour *et al.*, 2010), mechanistic models for C_3 (Buckley *et al.*, 2003; Rodriguez-Dominguez *et al.*, 2016) and C_4 plants (Bellasio *et al.*, 2017), knowledge of L_{NS} is sparse. L_{NS} are generally captured by empirical functions that act by reducing inputs of photosynthetic models as a function of water shortage (Vico & Porporato, 2008). Detailed knowledge of the onset and sensitivity of L_{NS} in response to dehydration and a meaningful comparison between C_3 and C_4 plants is therefore required to improve our mechanistic understanding of the processes underpinning L_{NS} and to quantify plant performance from leaves to ecosystem to global scales, in present, past, and future climatic scenarios.

We investigate L_{NS} in two C_3 crops (wheat and sunflower) and two C_4 crops (maize and sorghum) with a novel experiment whereby plants grown hydroponically were progressively drawn out of water forcing a fast but controlled dehydration. We derive a comprehensive suite of empirical and mechanistic photosynthetic parameters of healthy leaves, then measure assimilation, leaf water potential, stomatal conductance, and L_{NS} in response to dehydration. To isolate intraspecific and interspecific osmotic adjustment, we compare the onset of L_{NS} to the point of turgor loss. We provide fitted attenuation functions scaling model parameters to leaf water potential.

Materials and Methods

Plants

Seeds of *Zea mays* L., *Sorghum bicolor* (L.) Munch, *Helianthus annuus* L., and *Triticum aestivum* L., were germinated for a week on wet paper (C_4 seeds) or perlite (C_3 seeds). Twenty-litre black polypropylene tubs filled with water were fertilized with 150 cm^3 of Green Dream 1 complete fertilizer (Flairform, Applecross, Australia), supplemented with 2 g of Fe-EDTA for maize. Seedlings were transferred in foam rubber discs, and placed in 5-cm holes cut in the lids of the tubs. The solution was constantly aerated through aquarium stones, fertilized weekly with 50 cm^3 of the above fertilizer, and discarded after 3 wk. Plants were grown for 4–6 wk in controlled environment plant growth chambers (Thermoline Scientific, Wetherill Park, NSW, Australia), set at 26°C : 20°C (day : night), 80% relative humidity, with a 12-h photoperiod inclusive of a 9 h day (400 μmol m^{-2} s^{-1} at leaf level) interrupted by a 1-h midday peak illumination (690 μmol m^{-2} s^{-1} 1000 W metal halide arc lamps multi vapor® MVR; plus halogen, GE Lighting, East Cleveland, OH, USA), and flanked by 1-h dawn and 1-h dusk (80 μmol m^{-2} s^{-1} only halogen).

Hydromechanical characterization

A PSY1 psychrometer (ICT, Armidale, NSW, Australia), calibrated with five standard NaCl solutions according to the manufacturer's instructions, was used to measure leaf water potential. A small portion of epidermis (*c.* 3 × 1 mm) was removed with a razor blade from a fully expanded leaf of a plant standing in aerated water, rinsed repeatedly with abundant distilled water, then blotted with paper and fitted with the thermocouple of the PSY1, sealed with a tiny ridge of high vacuum grease following the manufacturer's instructions. Leaf water potential was measured every 10–20 min in the dark. When Ψ_L was constant (after 2–3 h), the leaf was cut at the base, sampled for the determination of osmotic potential, and placed on a balance together with the PSY1 mount. The initial tared weight was taken as turgid weight. Weight and Ψ_L were measured periodically throughout the day, then the leaf was removed and dried, and the weight of the PSY1 mount was recorded. Relative water content was calculated as:

$$RWC = 100\ \frac{\text{turgid weight} - \text{sample weight}}{\text{turgid weight} - \text{dry weight}}$$

The relationship between Ψ_L and RWC was simulated using the model of Bartlett *et al.* (2012). Briefly,

$$\Psi_L = \Psi_S + \Psi_P \qquad \text{Eqn 1}$$

where Ψ_S is the osmotic potential, Ψ_P here is pressure potential (the negative of turgor pressure).

Ψ_S was calculated as:

$$\Psi_S = \frac{\Psi_{S0}}{1 - R_S} \qquad \text{Eqn 2}$$

where Ψ_{S0} is the osmotic potential at full hydration, which was calculated from the measured bulk osmotic potential ($\Psi_{S\ Bulk}$), and the apoplastic water fraction (awf) as:

$$\Psi_{S0} = \Psi_{S\ Bulk}\left(1 + \frac{awf}{100}\right) \quad \text{Eqn 3}$$

and the apoplastic relative water content, R_S is:

$$R_S = 1 - \left(\frac{RWC - awf}{100 - awf}\right) \quad \text{Eqn 4}$$

Ψ_P was calculated as:

$$\Psi_P = \begin{cases} -\Psi_{S\,0} - \varepsilon\ R_S & \text{if} \quad -\Psi_{S\,0} - \varepsilon\ R_S > 0 \\ 0 & \text{else} \end{cases} \quad \text{Eqn 5}$$

where ε is the bulk elastic modulus, and other quantities are as defined above.

$\Psi_{S\ Bulk}$ was obtained as per Quirk *et al.* (2019a) by freezing and thawing leaves, then squeezing extracts onto 5-mm-diameter filter paper discs, inserted into the PSY1 mount and measured after 1 h.

Eqn 1 was calculated for all measured values of RWC and was iteratively fitted to the measured values of Ψ_L to estimate awf and ε. An example of the data and fitted curve is shown in Fig. 1, and fitted values are in Table 1.

Photosynthetic responses at full hydration

A portable gas exchange system (LI6400XT; Li–Cor, Lincoln, NE, USA) was modified to operate at low CO_2 concentrations (https://licor.app.boxenterprise.net/s/iv8ljrga3fjsqc4nrhti). Light was provided by a 6400–18 RGB light source, positioned to illuminate the leaf uniformly. Light intensity was measured by the gallium arsenide photodiode in the light source, removed from the light source and repositioned in the leaf chamber at leaf level, parallel to the leaf surface, and calibrated using a Li–250 light sensor (Li–Cor). Neoprene gaskets were used on both sides of the 3 cm × 2 cm cuvette. A mixture of 2% O_2 was prepared by mixing ambient air and N_2 with a bespoke gas mixing system. The synthetic air was humidified to a dew point of *c.* 14°C (C_3) or *c.* 17°C (C_4) upstream of the inlet to maintain a water vapour pressure deficit in the cuvette of *c.* 1 kPa. CO_2 was added from a cylinder (BOC, North Ryde, NSW, Australia), using the CO_2 injection unit of the LI6400XT. Plants were transferred to the laboratory the night before the experiment. A portion of a fully expanded leaf was clamped in the cuvette. In the morning, after photosynthetic induction under the photosynthetic photon flux density (PPFD) of 500 μmol m^{-2} s^{-1} and a reference (CO_2) of 300 μmol mol^{-1} for a minimum of 1 h, four photosynthetic response curves were measured at 25°C on each of $n = 4$ plants, A/C_i curves were measured under the PPFD of 500 μmol m^{-2} s^{-1}, light curves were measured under a reference (CO_2) of 420 μmol mol^{-1}, reproducing growth conditions. Flow rate was 490 μmol s^{-1}; CO_2 diffusion through the gaskets (Boesgaard *et al.*, 2013) was compensated by lengthening the tubing of the LI6400XT reference gas so that the additional diffusion through the supplemental tube in the reference line would match that of the sample line at a given flow rate (Bellasio & Farquhar, 2019).

Gas exchange data were analysed using the tools of Bellasio *et al.* (2016a,b). In short, the relationship between A and C_i for hydrated plants was modelled empirically as a nonrectangular hyperbola, describing assimilation (A_{mod}) for a given C_i after Prioul and Chartier (1977) as modified by Bellasio *et al.* (2016b):

$$A_{mod} = \frac{CE(C_i - \Gamma) + A_{SAT} - \sqrt{(CE(C_i - \Gamma) + A_{SAT})^2 - (4\omega A_{SAT} CE(C_i - \Gamma))}}{2\omega} \quad \text{Eqn 6}$$

where A_{SAT} represents the CO_2-saturated rate of A under the PPFD of the measurements and defines the horizontal asymptote. CE is carboxylation efficiency for CO_2 fixation, and defines the inclined asymptote. ω is an empirical factor ($\omega \neq 0$) defining curvature. Γ is the x-intercept, i.e. the C_i at which A is zero.

A complete set of mechanistic photosynthetic parameters was derived after Bellasio *et al.* (2016a,b), these procedures are briefly described in Supporting information Notes S1.

Photosynthetic responses to dehydration

We drove a rapid but controllable decrease in leaf water potential with an innovative dehydration experiment consisting of progressively pulling out of water roots of plants grown in hydroponics in several steps lasting *c.* 15 min, until leaves were irreversibly wilted. The evening before the experiment, plants were bagged in the dark and transferred to the laboratory. A fully expanded leaf was sampled for the determination of solute potential, and fitted with the PSY1 thermocouple as detailed in the Hydromechanical characterization section. An adjacent portion of the leaf was

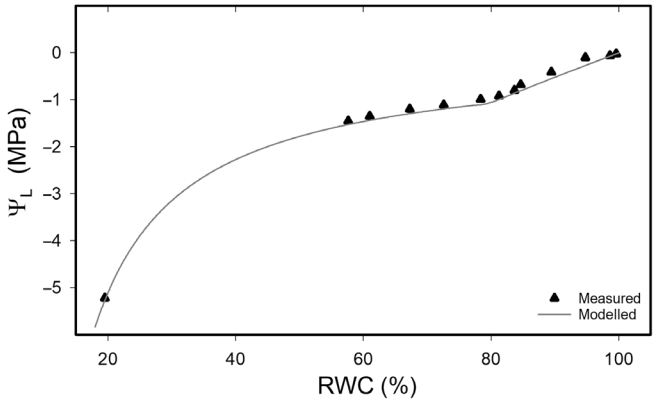

Fig. 1 Example of a pressure–volume curve obtained for sorghum. Pressure–volume curves were constructed by gravimetrically measuring the leaf relative water content (RWC) concurrently with the leaf water potential (Ψ_L) measured with a psychrometer. Triangles show the measured relative water content of the leaf, plotted against Ψ_L. The line represents the model output (Eqns 1–5) fitted to seven replicates concurrently to estimate the apoplastic water fraction (awf) and the bulk elastic modulus (ε).

New Phytologist

Table 1 Quantities derived from model fitting of pressure volume curves or exponential attenuation functions and associated statistics.

Description	Symbol	Unit	Maize	Sorghum	Wheat	Sunflower
From pressure volume curves						
Bulk leaf elastic modulus	ε	MPa	4.03 ± 0.41 (8)	5.53 ± 0.99 (7)	6.48 ± 0.68 (7)	4.07 ± 0.66 (7)
Apoplastic water fraction	awf	%	5.29 (8)	3.96 (7)	5.2 ± 2.7 (7)	10.3 ± 2.8 (7)
From J_a dehydration curves						
Shape of the attenuation function of J_a or J_{ATP}	*b*	MPa	0.914 ± 0.054 (15)	0.800 ± 0.076 (15)	1.87 ± 0.15 (12)	1.93 ± 0.44 (19)
Steepness of the attenuation function of J_a or J_{ATP}	*c*	MPa	0.192 ± 0.043 (15)	0.133 ± 0.024 (15)	0.26 ± 0.58 (12)	0.268 ± 0.061 (19)

Values are the average ± SE, and the number of biological replicates in brackets. The apoplastic water fraction (awf), which represents the extracellular water content diluting cytosolic osmolytes when cells are disrupted, was fitted separately for each replicate of wheat and sunflower, or, for sorghum and maize, it was fitted collectively across all replicates. This, along with the bulk elastic modulus (ε), which measures the degree of turgor loss due to a slight relative volume change, and therefore represents the rigidity of cell wall, were found through curve fitting, as described in Nadal *et al*. (2018). The attenuation function $J_d = \frac{J_h}{1+e^{-\frac{\Psi_{Soil}+b}{c}}}$ (Bellasio *et al*., 2017) was fitted either to J_a or J_{ATP}.

clamped in the LI6400XT and acclimated in the dark overnight with ambient air supply. A range of conditions was set with 21% (ambient) or 2% O_2 (to minimize photorespiration) and reference CO_2 concentrations of 300 μmol mol^{-1} that maximized the ratio between CO_2 concentration inside and outside the leaf (C_i/C_a), or 800 μmol mol^{-1} that minimized stomatal limitation. Flow rate was 490 μmol s^{-1} and PPFD was 500 μmol m^{-2} s^{-1}, reproducing growth PPFD. Assimilation and Ψ_L were recorded every 10–20 min. After complete photosynthetic acclimation (minimum 1 h), plants were progressively drawn out of the water, with the aim of reducing Ψ_L in steps of 0.1–0.15 MPa for each measurement period, until leaves were irreversibly wilted, after 6–8 h.

Stomatal and nonstomatal limitations

Stomatal limitation (L_S) was determined using Eqn 6, after Farquhar and Sharkey (1982) as:

$$L_S = \frac{A_h - A_p}{A_h} \quad \text{Eqn 7}$$

and nonstomatal limitation (L_{NS}) was calculated after Björkman *et al*. (1980) as:

$$L_{NS} = \frac{A_p - A_d}{A_h} \quad \text{Eqn 8}$$

where A_h is the potential A_{mod} that would occur in fully hydrated leaves if there were no stomatal impediment to CO_2 diffusion, calculated by setting $C_i = C_a$, the CO_2 concentration external to the leaf in the measurement cuvette, in Eqn 6. A_p is the potential A_{mod} of fully hydrated leaves, calculated by setting the measured C_i in Eqn 6, parameterised by fitting A/C_i response curves (Fig. 2), and A_d is the actual assimilation measured during dehydration (Fig. 3).

Modelling J_a or J_{ATP} and its attenuation

The rate of electron transport for C_3 plants was modelled by inverting a model of electron transport limited C_3 assimilation derived by Yin *et al*. (2009) after von Caemmerer and Evans (1991) based on Farquhar *et al*. (1980) as formulated by eqn 19 in Bellasio *et al*. (2016b), and by solving for J_a (solution is shown in Notes S2). For C_4 plants, the ATP production rate was modelled by inverting an ATP limited model of C_4 assimilation after von Caemmerer (2000) based on Berry & Farquhar (1978) as formulated in eqn 7 in Bellasio *et al*. (2017) and solving for J_{ATP} (solution is shown in Notes S2).

The attenuation of J_a (C_3) or J_{ATP} (C_4) was described using an exponential function from Osborne and Sack (2012) in the formulation of Bellasio *et al*. (2017) as:

$$J_d = \frac{J_h}{1 + e^{-\frac{\Psi_{Soil}+b}{c}}} \quad \text{Eqn 9}$$

where J_h is J_a calculated using eqn 12 in Bellasio *et al*. (2016b) (C_3) or J_{ATP} calculated using eqn 11 in Bellasio *et al*. (2016a) (C_4) using the parameterisation for well-watered conditions and operational PPFD and C_a (Table 2), *b* defines the slope of the attenuation, while *c* defines the shape of the sigmoidal curve.

Statistical analysis

Ψ_{CRIT} was identified by iteratively adjusting the cut-off between datapoints to maximize the combined R^2 of the split-line regression for each individual biological replicate. The hypothesis of water potential at turgor loss equalling the water potential at the incipient point of response ($\Psi_{TL} - \Psi_{CRIT} = 0$) was tested with a two-tail paired *t*-test using the data analysis pack of Excel®. S_Ψ was subject to a one-way ANOVA with species as a fixed factor and a Tukey multiple comparison test for $P = 0.05$ (Genstat® 18.2; VSNI, Hemel Hempstead, UK).

Results

Hydromechanical characterisation

The bulk elastic modulus (ε, that is, the stiffness of cell walls), which was *c*. 5 MPa, irrespective of the species, and the apoplastic water fraction (awf, that is, that fraction of leaf water not contained by the plasmalemma), which ranged between 4% in sorghum and 10% in sunflower, are shown in Table 1.

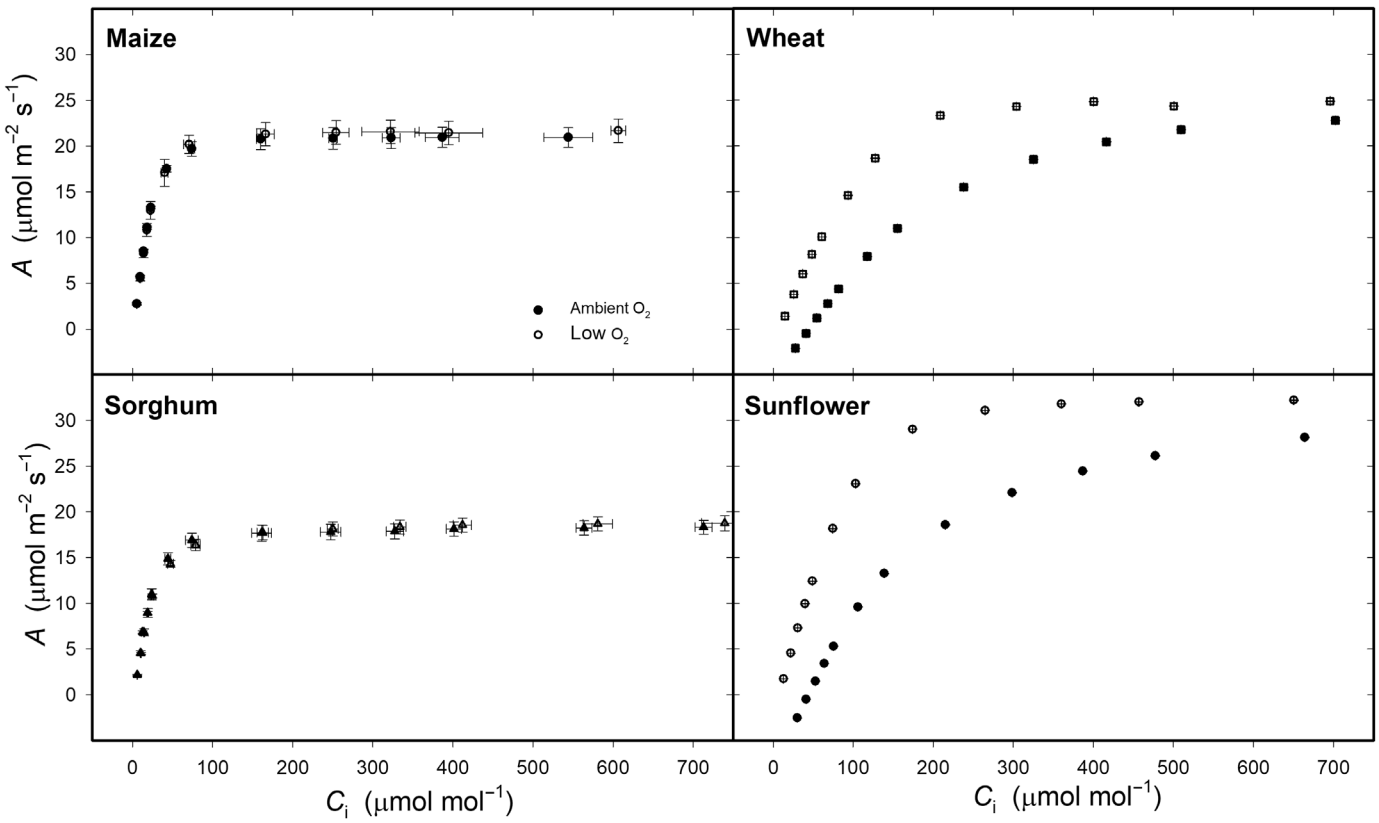

Fig. 2 Response of assimilation to CO_2 concentration in the substomatal cavity (A/C_i curves). Responses were measured under ambient O_2 concentration (filled symbols) or under low O_2 concentration (empty symbols) at a light intensity of 500 μmol m^{-2} s^{-1}, on fully hydrated maize (top left), wheat (top right), sorghum (bottom left), or sunflower (bottom right) leaves. $n = 4$ biological replicates for each species. Error bars show ± SE for A and C_i.

Assimilatory responses at full hydration

Assimilation of fully hydrated plants measured with roots standing in aerated water in response to stepwise variations in light intensity (PPFD) and CO_2 concentration in the measurement cuvette, under both ambient and low O_2 concentrations, were typical for healthy C_3 and C_4 plants (A/C_i curves measured under ambient (O_2) are shown in Fig. 2, A/PPFD curves measured under ambient (O_2) as well as A/C_i and A/PPFD curves measured under low (O_2) are not shown, but data are available in File S2). The trend of these responses was captured by fitting empirical hyperbolas, which do not require specific assumptions about the underpinning physiology and were therefore used for the subsequent limitation analysis for both C_3 and C_4 plants. Fitted parameters are shown in Table 2, fitted curves are plotted in Fig. 3. Additionally, we fitted common mechanistic models to derive a comprehensive set of photosynthetic parameters, using the framework of Bellasio *et al.* (2016b) for C_3 plants and that of Bellasio *et al.* (2016a) for C_4 plants, shown in Table 2.

Gas exchange during dehydration

In day-long experiments, after photosynthesis stabilized, plants were pulled out of the water in several steps until leaves were irreversibly wilted, resulting in the primary traces of assimilation rate plotted against leaf water potential (Ψ_L) shown in Fig. 4a for C_4 maize and sorghum and 4B for C_3 wheat and sunflower. To resolve L_{NS}, each paired CO_2 concentration in the substomatal cavity (C_i) and assimilation (C_i, A) was then compared with the modelled A/C_i curves at full hydration (Fig. 3). Any pair lying on the modelled curves will have zero L_{NS} (point h in Fig. 3). L_{NS} will commence as (C_i, A) progressively dips below the curves (point d in Fig. 3). When L_{NS} was plotted against Ψ_L, L_{NS} was negligible until a sharp inflection point, and rose rapidly at more negative Ψ_L both for C_4 maize and sorghum (Fig. 5c) and C_3 wheat and sunflower (Fig. 5d). We derived rates of electron transport and ATP production for each measured value of A_{OP} and $C_{i\ OP}$. Example primary traces are shown in Fig. 5e,f for C_4 and C_3 plants, respectively. We fitted exponential attenuation functions (Eqn 9) for each individual replicate of each species. Fitted values are shown in Table 1. The functions were similar within C_4 maize and sorghum and C_3 wheat and sunflower, and we therefore plotted the averages in Fig. 5e,f. The attenuation was steeper and dropped at a less negative Ψ_L in C_4 maize and sorghum than in C_3 wheat and sunflower.

Two regression lines were fitted to the linear portion of L_{NS} (Fig. 6a) or L_W left and right of the inflection. The value of Ψ_L at the intersection was termed the critical water potential (Ψ_{CRIT}), while the slope of the regression line right of Ψ_{CRIT} is sensitivity of L_{NS} to water potential, $S(L_{NS})_\Psi$, where $S(L_{NS})_\Psi = \frac{d\,L_{NS}}{d\,\Psi_L}$ (Fig. 6a), or of L_W $S(L_W)_\Psi = \frac{d\,L_W}{d\,\Psi_L}$ (Fig. 6b).

New Phytologist

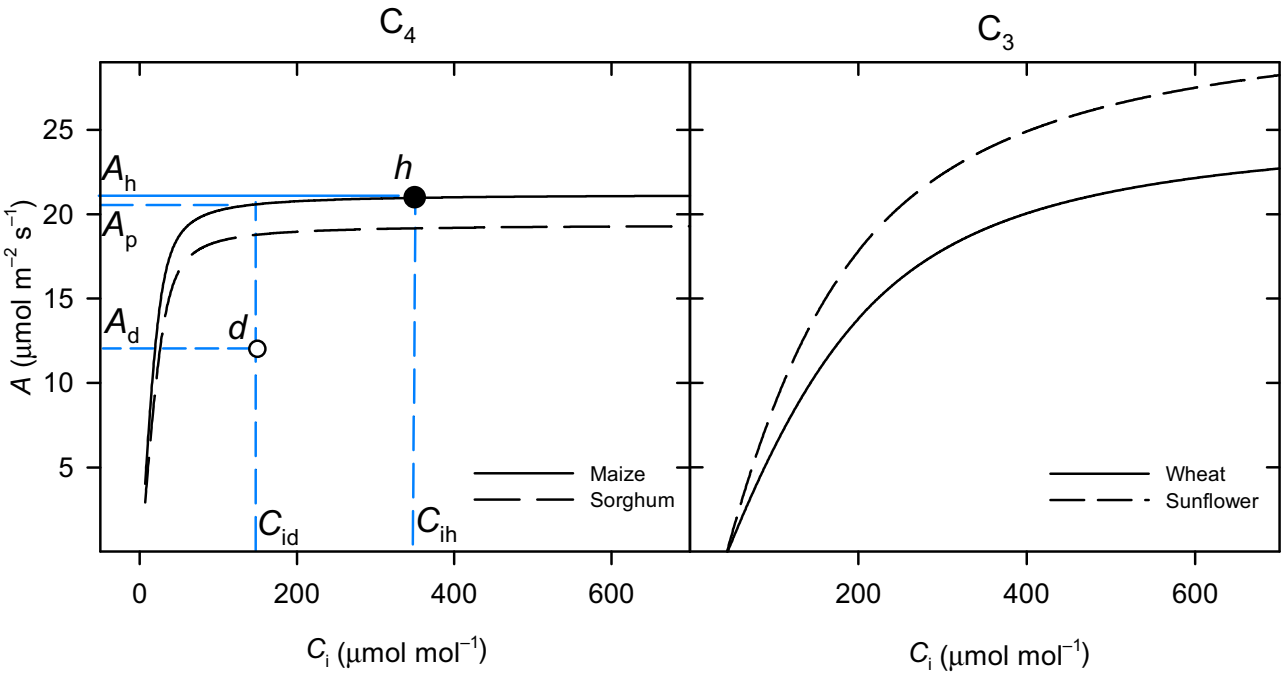

Fig. 3 Fitted A/C_i curves and calculation of nonstomatal limitation. The black lines show the average curves for four species empirically fitted to the assimilation rate (A) of fully hydrated plants, plotted against CO_2 concentration in the substomatal cavity (C_i, raw curves are plotted in Fig. 2). The calculation of nonstomatal limitation (L_{NS}) and stomatal limitation (L_S) for C_4 assimilation is exemplified with maize. The point h represents a typical pair (C_{ih}, A_h) measured at full hydration under a C_a of 800 μmol mol^{-1} and growth light intensity of 500 μmol m^{-2} s^{-1}. The point d represents a typical pair (C_{id}, A_d) measured under dehydration. The potential assimilation that a hydrated plant would have at C_{id} is called A_p. The difference between A_h and A_p, relative to A_h, is L_S; the difference between A_p and A_d, relative to A_h, is L_{NS}.

To isolate intraspecific and interspecific differences in osmotic potential (Ψ_S), for each individual plant, we compared Ψ_{CRIT} with water potential at turgor loss (Ψ_{TL}, estimated from Ψ_S using awf and ε in Table 1). Ψ_{CRIT} was significantly greater than Ψ_{TL} in C_4 maize and sorghum, both when calculated for L_{NS} (Fig. 6c) and L_W (Fig. 6d), while Ψ_{CRIT} did not significantly differ from Ψ_{TL} in C_3 wheat and sunflower. We term the positive difference ($\Psi_{CRIT} - \Psi_{TL}$) the residual water potential (Ψ_R). This was negligible for C_3 wheat and sunflower, and as large as 0.4 MPa for maize, and 0.2 MPa in sorghum.

The sensitivity of L_{NS} and L_W to Ψ_L can be directly compared across plants. C_4 maize and sorghum had a nearly threefold greater $S(L_{NS})_\Psi$ than C_3 wheat and sunflower had (Fig. 6e), while $S(L_W)_\Psi$ was higher in sorghum than in sunflower (Fig. 6f).

Discussion

We set out to compare the rise of L_{NS} in response to rapid dehydration between two C_4 and two C_3 crops. Although we previously worked with undomesticated grasses (Bellasio *et al.*, 2022), we chose these crops for their economic relevance, and for the high uniformity between replicates that reduced experimental error. In the laboratory, we exposed plants to a constant illumination (through a LED canopy light) and air humidity (that of the laboratory) while varying the wind speed (with a table fan) and plant water supply. To do that, we reduced the proportion of roots that were submerged in water (Fig. S1), with the target of obtaining a gradient of reduction of Ψ_L of 0.1 MPa every 15 min. This imposed a controllable dehydration at higher rate than in conventional drought experiments, where water limitation is obtained over the course of days. This allowed us to focus on the primary effect of dehydration ('strain') over the secondary responses that plants deploy to counter the stress ('tolerance') presumably taking a longer time to deploy.

The approach used to identify nonstomatal limitation (L_{NS}) relies on the accuracy with which intercellular CO_2 concentrations (C_i) are estimated. The heterogeneity in stomatal conductance (g_S) due to nonuniformity in density, distribution, and opening across the leaf surface, called patchiness, may impact the accuracy of C_i calculation, and may be exacerbated by dehydration. Unfortunately, a direct method to measure the effect of patchiness does not exist (Pospíšilová & Šantrůček, 1994). In our opinion, Downton *et al.* (1988) overestimated the effect of patchiness by incorrectly assuming that any decrease in PSII yield during dehydration was solely due to a reduction in C_i, thus neglecting the contribution of L_{NS}. More realistically, in a comprehensive theoretical study, Buckley *et al.* (1999) concluded that the impact of patchiness was often minimal, especially when stomatal aperture followed a normal distribution (rather than being either fully open or fully closed) and when leaves were 'highly coupled' to the surrounding air. These conditions were likely present in our measurements, where g_S was relatively high (Fig. 4c, d), boundary layer conductance and thermal gradients were minimised due to vigorous ventilation, transpiration was relatively

Table 2 C_4 photosynthesis parameters obtained from curve fitting of gas exchange responses.

				Maize		Sorghum		Wheat		Sunflower	
O_2	Symbol	Unit	Description	Mean	SE	Mean	SE	Mean	SE	Mean	SE
21%	R_{LIGHT}	μmol m^{-2} s^{-1}	Respiration in the light[a]	1.19	0.096	0.928	0.069	0.727	0.075	1.13	0.070
2%	R_{LIGHT}	μmol m^{-2} s^{-1}	Respiration in the light[a]	1.13	0.18	1.10	0.049	0.914	0.060	1.37	0.12
21%	$Y(II)_{LL}$	dimensionless	Initial yield of PSII extrapolated to PPFD = 0[a]	0.675	0.0087	0.741	0.0058	0.709	0.0060	0.792	0.0041
2%	$Y(II)_{LL}$	dimensionless	Initial yield of PSII extrapolated to PPFD = 0[a]	0.649	0.0077	0.758	0.0068	0.697	0.029	0.768	0.0049
21%	*LCP*	μmol m^{-2} s^{-1}	Light compensation point, i.e. PPFD when $A = 0$[b]	23.2	2.1	21.3	1.2	15.3	1.6	20.2	1.2
21%	$PPFD_{50}$	μmol m^{-2} s^{-1}	PPFD that half saturates *GA*[b]	421	13	721	60	446	10	423	23
21%	$Y(CO_2)_{LL}$	CO_2/quanta	Quantum yield for CO_2 fixation, that is quanta required for each CO_2 assimilated, extrapolated to PPFD = 0; also known as Φ_{CO2LL}[b]	0.0519	0.0032	0.0437	0.0014	0.0479	0.00086	0.0561	0.00052
21%	GA_{SAT}	μmol m^{-2} s^{-1}	Light-saturated *GA*, under the CO_2 concentration of light curves[b]	37.1	2.3	49.3	4.2	34.4	0.56	40.8	2.5
21%	*m*	dimensionless	Curvature of the nonrectangular hyperbola describing the PPFD dependence of *GA*[b]	0.823	0.032	0.720	0.043	0.758	0.022	0.835	0.015
2%	*LCP*	μmol m^{-2} s^{-1}	Light compensation point[b]	21.1	2.4	24.0	0.81	14.7	0.98	19.0	1.5
2%	$PPFD_{50}$	μmol m^{-2} s^{-1}	PPFD that half saturates *GA*[b]	432	7.62	894	94	437	19	394	11
2%	$Y(CO_2)_{LL}$	CO_2/quanta	Quantum yield for CO_2 fixation[b]	0.0532	0.0041	0.0465	0.0010	0.0627	0.0011	0.0721	0.0011
2%	GA_{SAT}	μmol m^{-2} s^{-1}	Light-saturated *GA*[b]	39.1	2.7	56.2	4.0	44.9	1.5	50.9	1.3
2%	*m*	dimensionless	Curvature of the hyperbola[b]	0.827	0.017	0.530	0.080	0.782	0.033	0.885	0.025
21%	CE	mol m^{-2} s^{-1}	Carboxylation efficiency, that is initial slope of the A/C_i curve[b]	0.800	0.052	0.606	0.054	0.123	0.0019	0.182	0.0082
21%	A_{SAT}	μmol m^{-2} s^{-1}	CO_2-saturated *A*, under the PPFD of A/C_i curves[b]	21.2	1.2	18.3	0.83	25.6	0.40	32.5	0.63
21%	ω	dimensionless	Curvature of the nonrectangular hyperbola describing the C_i dependence of *A*[b]	0.857	0.0091	0.877	0.012	0.670	0.038	0.511	0.033
21%	Γ	μmol mol^{-1}	C_i–A compensation point, that is C_i at which $A = 0$[b]	1.80	0.088	2.07	0.49	44.7	0.36	43.9	0.27
2%	CE	mol m^{-2} s^{-1}	Carboxylation efficiency[b]	0.720	0.057	0.770	0.058	0.196	0.013	0.327	0.027
2%	A_{SAT}	μmol m^{-2} s^{-1}	CO_2-saturated *A*[b]	21.8	1.3	19.0	0.84	25.4	0.48	33.2	0.85
2%	ω	dimensionless	Curvature of the hyperbola[b]	0.895	0.0072	0.577	0.078	0.914	0.016	0.859	0.023
2%	Γ	μmol mol^{-1}	C_i–A compensation point[b]	1.33	0.18	2.71	0.059	6.30	0.55	7.27	0.27
2%	*s* (C_3) *s′* (C_4)	$Quanta^{-1}$	Combined conversion efficiency of incident light into e^- (C_3) (Yin *et al*., 2004) or ATP (C_4) (Yin *et al*., 2011)[a]	0.254	0.012	0.202	0.0029	0.365	0.018	0.401	0.0055
21%	J_{SAT} or J_{ATPSAT}	μmol m^{-2} s^{-1}	Light-saturated e^- (C_3) or ATP (C_4) production rate[c]	216	18	284	19	190	17	237	9.6
21%	θ	dimensionless	Curvature of the nonrectangular hyperbola describing the PPFD dependence of J_{ATP}[c]	0.798	0.034	0.635	0.066	0.732	0.037	0.801	0.022
21%	g_M or g_{BS}	mol m^{-2} s^{-1}	M (C_3)[d] or BS (C_4)[e] conductance to CO_2 diffusion	0.00221	0.00049	0.00252	0.00024	0.766	0.41	0.433	0.058
21%	V_{CMAX} or V_{PMAX}	μmol m^{-2} s^{-1}	Maximum Rubisco (C_3)[f] or PEPC (C_4)[g] carboxylation rate[d]	123	13	52.1	2.3	101	1.1	165	6.0

Gas exchange data of C_3 plants were analysed with the protocol and workbook of (Bellasio *et al*., 2016b), and, for C_4 plants with those of Bellasio *et al*. (2016a). To derive BS conductance for C_4 plants we used the model of von Caemmerer (2000) with the procedure described in Yin *et al*. (2011), after Bellasio and Griffiths (2014a). $n = 4$ biological replicates.

[a]Linear fitting of gas exchange and fluorescence (Yin *et al*., 2011) following (Bellasio *et al*., 2016b) (C_3) and Bellasio *et al*. (2016a) (C_4).

[b]Fitted nonrectangular hyperbola (Bellasio *et al*., 2016b).

[c]Nonlinear calibration of Bellasio and Griffiths (2014a).

[d]Concurrent fitting of A/C_i and light curves under light limited conditions using non-linear estimates of J_{ATP} using the model of von Caemmerer (2000), following Bellasio and Griffiths (2014a) and Bellasio *et al*. (2016a).

[e]Concurrent fitting of light and A/C_i curves in the light limited region, using a point calibration for J_a, RLIGHT under 2% O_2, SC/O from the curve fitting procedure of Yin *et al*. (2009), all following Bellasio *et al*. (2016b).

[f]Fitting the model of von Caemmerer and Furbank (1999), following Bellasio *et al*. (2016a).

[g]Fitting the model of Ethier and Livingston (2004), following Bellasio *et al*. (2016a,b).

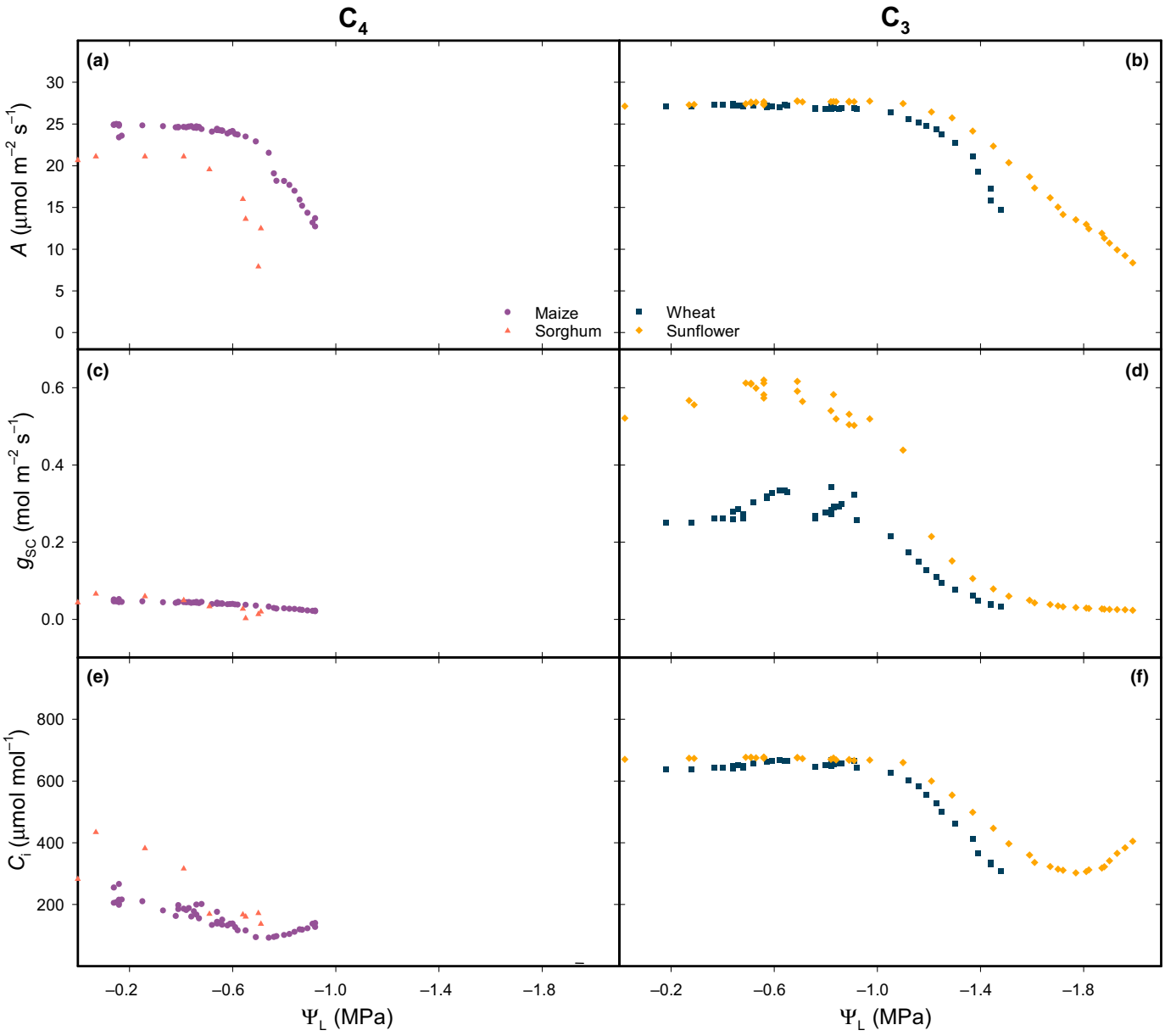

Fig. 4 Gas exchange under rapid dehydration. C_4 maize and sorghum (left) and C_3 wheat and sunflower (right) plants grown in hydroponics were progressively drawn out of the water while water potential (Ψ_L) and gas exchange were measured every 10 min (*c.* 30 min for sorghum). Panels (a, b) example of primary traces of assimilation (*A*); panels (c, d), stomatal conductance to CO_2 (g_{SC}); panels (e, f), CO_2 concentration in the substomatal cavity (C_i).

low (*c.* 2 mmol m^{-2} s^{-1} for C_4 maize and sorghum and 3 mmol m^{-2} s^{-1} for C_3 wheat and sunflower), and irradiance in the IRGA leaf cuvette was moderate (500 μmol m^{-2} s^{-1}). Indeed, circumstantial evidence suggests that patchiness either did not occur or had an insignificant impact on our findings. First, stomatal patchiness is typically associated with fluctuations in C_i measured by the IRGA (Mott & Buckley, 1998), which we did not observe. Second, if stomatal patchiness were to cause a significant misestimation of C_i, then Ψ_{CRIT} would depend on the method used to calculate L_{NS}. However, this was not the case in our study. Ψ_{CRIT} derived for L_{NS} (Fig. 6c), followed the same patterns as Ψ_{CRIT} derived for L_W, which is directly derived from measured assimilation values without relying on C_i. Additionally, separate paired *t*-tests comparing Ψ_{CRIT} (L_{NS}) = Ψ_{TL} obtained under elevated or low CO_2 concentrations yielded similar results to the pooled data. Third, $S(L_{NS})_\Psi$ would be influenced by C_i, meaning that $S(L_{NS})_\Psi$ obtained under low C_i would differ from $S(L_{NS})_\Psi$ obtained under elevated C_i. Contrarily, our study did not reflect this situation. An ANOVA that included CO_2 level as a fixed factor found no significant effect of CO_2 level ($P = 0.91$), nor its interaction with species ($P = 0.94$) on $S(L_{NS})_\Psi$.

A second potential source of error lies in the uncertainties affecting measurements of Ψ_L. Pressure chamber measurements, used in our previous experiments, were not a suitable alternative

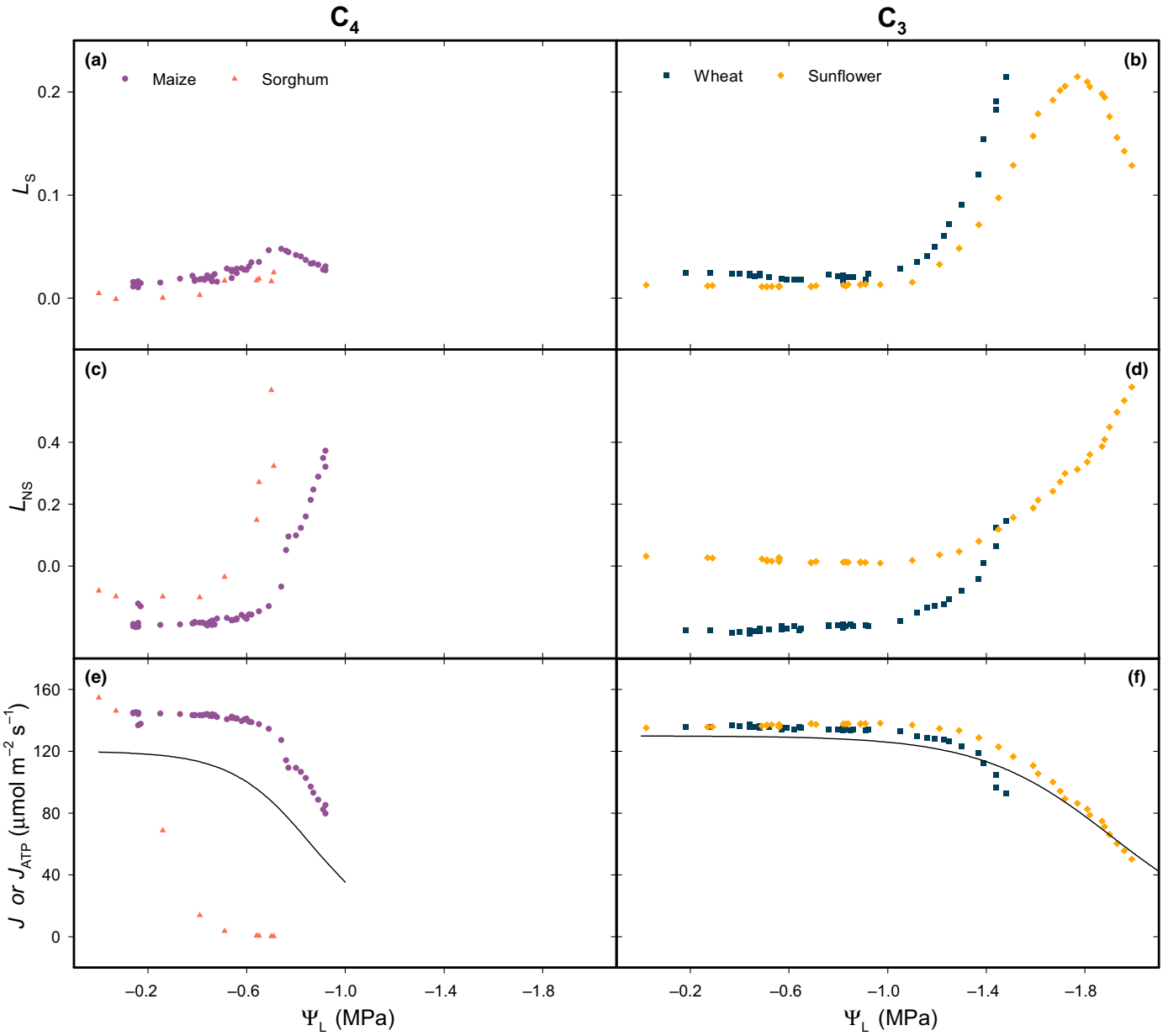

Fig. 5 Analysis of limitations and electron transport. Example of primary traces obtained for stomatal limitation (L_S) in panels (a, b), and nonstomatal limitation (L_{NS}), panels (c, d) were calculated using the parameters in Table 2, and visualized in Fig. 3, obtained by curve fitting to the measured A/C_i curves shown in Fig. 2. Rates of electron transport calculated for C_3 plants, and rates of ATP generation calculated for C_4 plants are shown in panels (e, f), respectively. Black lines show an exponential attenuation function (Eqn 9) obtained by averaging the coefficients fitted to the data obtained for each individual biological replicate ($n = 15$ for sorghum and maize, $n = 12$ for wheat and $n = 19$ for sunflower).

here because they are destructive and cannot be made continuously. The need to sample leaf portions progressively closer to the gas exchange cuvette as drought advances would possibly introduce an artefactual hydration gradient between the earliest and the latest samples and could potentially pose the risk of running out of leaf blade to cut in longer lasting experiments. Additionally, maize or sorghum or sunflower leaves are normally broader than the pressure chamber gasket and would need to be cut into longitudinal strips. This would mean introducing into the pressure chamber a rectangle of leaf cut on all four sides, where the presence of leaf cell sap and bubbles generated by the air coming in from the cuts would mask the squeezed sap and make it difficult to detect the equilibrium point. Psychrometry, which was selected as the only viable option to monitor Ψ_L in real time, has two other potential sources of error. First, the lateral heterogeneity between the site of Ψ_L measurement and gas exchange. The thermocouple is sealed on the leaf, which suppresses transpiration in that area, allowing the psychrometer to equilibrate with the leaf vein xylem water rather than the mesophyll of the transpiring parts of the leaf. Second, cutting a window of epidermis results in the spillage of cell sap. This may lower the osmotic potential at the psychrometer thermocouple resulting in an overestimation of

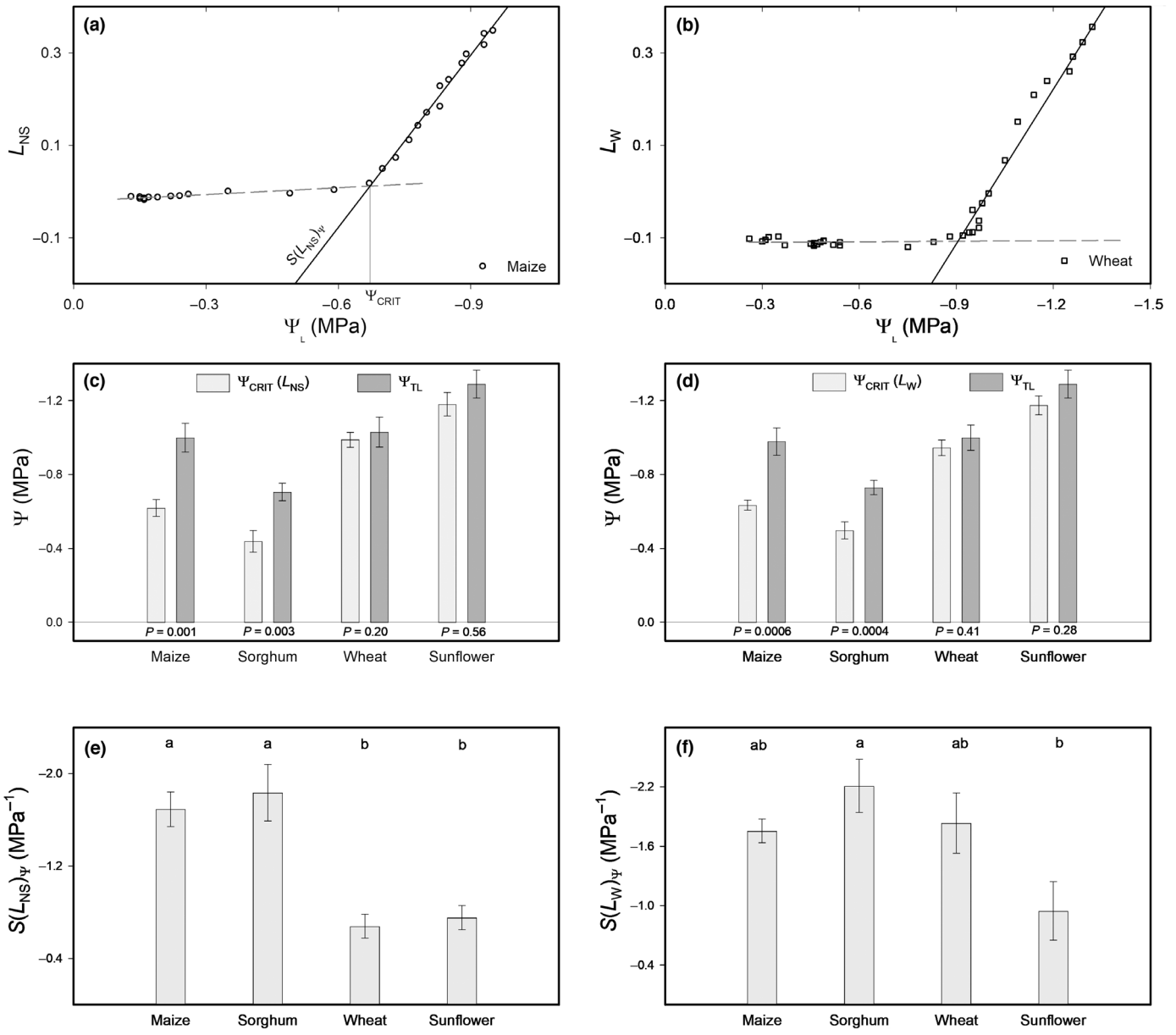

Fig. 6 Leaves of C_4 maize and sorghum are more susceptible to dehydration than C_3 wheat and sunflower. Panel (a) shows an example response of non-stomatal limitations L_{NS} obtained for maize, by calculating for each measured assimilation (represented by the traces shown in Fig. 4a) – and the corresponding CO_2 concentration in the substomatal cavity (C_i, shown in Fig. 4c) – the relative vertical distance from the A/C_i curves of fully hydrated plants shown in Fig. 3 (left). A split-line regression was fitted individually to each replicate, the Ψ_L of the intersection was taken as Ψ_{CRIT}, and the slope of the regression right of Ψ_{CRIT} is the sensitivity to water potential, $S(L_{NS})_\Psi$. An example of analogous derivation of sensitivity of water limitation, $S(L_W)_\Psi$, in wheat is shown in Panel (b). Comparison between Ψ_{CRIT} (L_{NS}) or Ψ_{CRIT} (L_W) and the water potential at turgor loss (Ψ_{TL}) for the four species are shown in panels (c, d), respectively. Ψ_{TL} was estimated for each sample by measuring the bulk osmotic potential on the same leaf that was undergoing gas exchange measurements, and correcting for apoplastic water fractions and bulk elastic modulus, previously determined (Fig. 1; Table 1). *p*-values were obtained in a two-tail paired *t*-test for a null hypothesis of $\Psi_{CRIT} = \Psi_{TL}$. Panel (e) show the average sensitivity of L_{NS} to water potential, $S(L_{NS})_\Psi$, and Panel (f) the analogous sensitivity of L_W, $S(L_W)_\Psi$, for the four species, obtained as shown in panels (a, b). Bars with the same letters were not different in a Tukey multiple comparison at a $P = 0.05$. Error bars show ± SE; maize $n = 10$, sorghum $n = 14$, sunflower $n = 17$, and wheat $n = 12$ biological replicates.

Ψ_L. Spillage is inevitable because it is necessary to have the thermocouple sense the water status of the leaf, and this requires removing the epidermis. We took precautions to counter spillage by rinsing and blotting the wound thoroughly and repeatedly, and by leaving the leaf to recover overnight, to allow viable cells to recapture spilled osmolytes. In addition, to avoid any systematic bias, we estimated the turgor loss point also with the same 'window' technique and then by curve fitting pressure volume curves.

We computed sensitivity to dehydration, as the relative decrease in a variable (*e.g.* L_W, L_{NS}, A) caused by a small decrease in water potential. Mathematically, $S(L_W)_\Psi$ represents the derivative of L_W's response to Ψ_L (initially during dehydration, it is equivalent to $\frac{dLn\,(A)}{d\Psi_L}$), and is generally unrelated to the value of

the assimilation variable. In the literature, the concept of drought sensitivity is often confused with that of a low average value of assimilation under drought. However, it is flawed to assume that a plant is more drought-sensitive simply because it has a lower assimilation rate (alternatively, sturdy plants may grow slower). For instance, the observation of Taylor *et al.* (2014) that 'C_4 always outperformed C_3 in these sister grass species, particularly under drought' is not directly telling that C_3 grasses are more drought-sensitive. To draw an analogy, when comparing brakes in an economy car and a race car, it would be misleading to simply observe that the economy car is driving at a slower speed at a specific moment. Instead, one has to compare the percentage decline in speeds when both drivers apply the brakes.

We found that L_{NS} commenced at a water potential $\Psi_{CRIT,}$ which was much less negative in C_4 maize and sorghum than C_3 wheat and sunflower. That positive difference between turgor loss and Ψ_{CRIT}, which we termed residual water potential Ψ_R, measured 0.4 MPa in maize and 0.2 MPa in sorghum – roughly double and comparable to the air pressure in a car tire. As dehydration progressed, and Ψ_L became more negative than Ψ_{CRIT}, the rate of increase in L_{NS}, or the sensitivity of L_{NS} to dehydration, $S(L_{NS})_\Psi$, was three times higher in C_4 maize and sorghum compared to that in C_3 wheat and sunflower (Fig. 6c). There is abundant evidence supporting our findings.

In laboratory conditions, using excised leaf discs from 76 species, Takeda and Fukiyama (1981) and Takeda *et al.* (1983) obtained remarkably notable results. They measured photosynthesis with a liquid phase O_2 electrode, regulating the osmotic potential by addition of sorbitol to the buffer after Xu *et al.* (1990), and calculated the water potential at 50% photosynthetic depression (Ψ_{50}). In 19 C_3 grass species from six subfamilies, the average Ψ_{50} was −3.75 MPa, much lower than the average Ψ_{50} of −1.29 MPa averaged over seven C_4 NADP-ME species and −2.36 MPa averaged over seven NAD-ME or PEPCK species. Similar results were found for Cyperaceae species from five tribes of three subfamilies, where Ψ_{50} averaged −3.91 MPa for 27 C_3 species and −1.78 MPa for 16 C_4 species.

In controlled conditions, we previously showed that three non-domesticated C_4 grasses, *Themeda triandra*, *Heteropogon contortus*, and *Eragrostis curvula*, were all sensitive to rapid fluctuations of water availability that did not affect C_3 plants (Quirk *et al.*, 2019b). Carmo-Silva *et al.* (2007) showed strong photosynthetic downregulation in three C_4 grasses with different decarboxylating mechanisms, subject to the addition of polyethylene glycol to the nutrient solution 20–26 h before measurements. Comparative studies of related C_3 and C_4 grasses show that C_4 species experience greater reductions in photosynthetic rates during drought compared with C_3 species both in controlled (Taylor *et al.*, 2011) and in common garden conditions (Ripley *et al.*, 2007, 2010). Ward *et al.* (1999) found, in a pot study, that the sensitivity of assimilation to dehydration was 136% higher for C_4 *Amaranthus retroflexus* than for C_3 *Abutilon theophrasti*.

In the field, Taylor *et al.* (2014) found that C_4 assimilation dipped correspondingly with midday depressions of leaf water potential, while, in C_3 species, assimilation decreased slower and paired with g_S and predawn water potential, consistent with evidence from their previous experiments in controlled conditions. Under natural conditions in a dry-sites transect – performed from the Xinjiang steppes to the Taklamakan desert, in China – under relatively mild drought conditions, five native C_4 species both monocot and dicot presented much more strongly depressed assimilation rates than co-occurring 18 native C_3 species, with the sole exception of C_4 *Setaria viridis* (Flexas *et al.*, 2022). One of the C_4 species showing large photosynthetic depression in that study was *Atriplex tatarica*, and indeed Rakhmankulova *et al.* (2019) had previously found a greater L_W in C_4 *Atriplex tatarica* than in the closely related C_3 *Atriplex verrucifera* over a 4-d water stress treatment.

It has been long known, based on those prior studies, that C_4 plants maintain a higher ratio of leaf water supply relative to demand (Quirk *et al.*, 2019b), which was previously theorized to provide a primary evolutionary advantage for C_4 plants (Osborne & Sack, 2012). However, here, we showed in maize and sorghum that the high ratio of water supply relative to demand was necessary to maintain the required hydration margin Ψ_R; in its absence, photosynthetic assimilation abruptly declined.

The physiological reasons for maintaining a residual Ψ_R are unknown. A possible explanation is that additional tension may be required to drive the flux of water out of the vasculature. The outside-xylem hydraulic conductance was reported to be much lower in C_4 *Panicum antidotale* than in C_3 *Panicum bisulcatum* measured by Sonawane *et al.* (2021). We interpret this by the fact that in C_4 plants, water flow between M and BS cells is entirely symplastic, constrained through plasmodesmata by the suberization of the middle lamella. Additional tension would be required to deliver water from the xylem to the mesophyll, through this symplastic constriction. However, we did not quantify outside-xylem hydraulic conductance, leaving uncertainty about whether in our plants Ψ_R solely consists of this overtension or if it also encompasses residual turgor pressure within the mesophyll.

When leaf water potential dropped below the Ψ_{CRIT} threshold, sensitivity of nonstomatal limitation to dehydration $S(L_{NS})_\Psi$ was three times higher for maize and sorghum than for wheat and sunflower. Similar results, described above, were obtained by Takeda *et al.* (1983) exploring a diverse range of wild species. The liquid phase method Takeda *et al.* (1983) used in their study bypassed the limitations imposed by stomatal conductance (Ishii *et al.*, 1977), and allowed the water potentials in the M, the xylem, and the BS to equilibrate. This suggests that the mechanism leading to a low Ψ_{CRIT} and high $S(L_{NS})_\Psi$ may be, at least in good part, independent of water delivery to mesophyll cells, and may reflect an inherent short-term susceptibility of the bicellular C_4 system.

Under dehydration, cytosol solute concentration increases passively, and for the active accumulation of sugars and amino acids such as proline (Rakhmankulova *et al.*, 2019), resulting in an increase in cytosol viscosity. This is possibly accompanied by a turgor-mediated decrease in the cross-sectional area of plasmodesmata. In C_4 plants, both these effects could potentially hinder intercellular transport between M and BS cells. Achieving high rates of C_4 assimilation requires sharing of metabolic functions

between the M and BS, and the rapid exchange of metabolites must be maintained between the two (Bellasio & Griffiths, 2014b; Bellasio & Lundgren, 2016; Bellasio, 2017). We propose that a high $S(L_{NS})_\Psi$ would be due to the slowdown of metabolite exchange, which would impede an essential component of the C_4 mechanism. If the high Ψ_R observed in maize and sorghum comprises a turgor component, this might serve to keep plasmodesmata connectivity above a minimum threshold.

Conclusion

Under rapid dehydration, assimilation had a steeper decrease in C_4 maize and sorghum than in C_3 wheat and sunflower due to nonstomatal limitation. Rapid declines in assimilation were previously observed in numerous C_4 species in in both laboratory and natural settings. Therefore, we infer that this sensitivity to dehydration could result from the disruption of an inherent feature of C_4 bicellular photosynthesis. We hypothesize that an hindrance to metabolite transport between M and BS cells might be the cause.

Acknowledgements

We thank John Passioura, for help with experimental design; Ichiro Terashima for sourcing from the library and translating Japanese two articles that greatly enriched our discussion; to Professor Osamu Ueno and The Crop Science Society of Japan for authorising articles reprint (articles are now openly accessible from Zenodo and the UCD institutional repository); Meisha-Marika Holloway-Philips, and Nerea Ubierna for spreadsheets; Hipolito Medrano, Colin Osborne, Susanne von Caemmerer, and Dean Price for equipment; Illa Tea for review; Suan Chin Wong for sweet words of encouragement, technical assistance, and seeds; Marc Carriquí for demonstrating methods to us; Richard Richards, Davide Gusberti, and Ross Deans for seeds; Florian Busch and Michael Roderick for discussion. We owe gratitude to reviewers for the time taken to deeply understand our work, and the detail of the constructive comments that have substantially contributed to improving the manuscript. We gratefully acknowledge funding from European Union's Horizon 2020 research and innovation programme through an MSCA (grant agreement ID no: 702755) and through a Science Foundation Ireland Individual Pathway Fellowship (21/PATH-S/9322), both fellowships awarded to CB. Open access publishing facilitated by Australian National University, as part of the Wiley - Australian National University agreement via the Council of Australian University Librarians.

Competing interests

None declared.

Author contributions

CB conceived the project, acquired funding and designed the experiment with contributions from JF. GDF provided laboratories and resources. CB performed the research with contributions of HS-W. CB analysed the data. CB, HS-W, JF and GDF wrote the paper.

ORCID

Chandra Bellasio https://orcid.org/0000-0002-3865-7521
Graham D. Farquhar https://orcid.org/0000-0002-7065-1971
Jaume Flexas https://orcid.org/0000-0002-3069-175X
Hilary Stuart-Williams https://orcid.org/0000-0002-9272-9178

Data availability

All data are included in the Supporting Information.

References

Bartlett MK, Scoffoni C, Sack L. 2012. The determinants of leaf turgor loss point and prediction of drought tolerance of species and biomes: a global meta-analysis. *Ecology Letters* **15**: 393–405.

Bellasio C. 2017. A generalised stoichiometric model of C_3, C_2, $C_2 + C_4$, and C_4 photosynthetic metabolism. *Journal of Experimental Botany* **68**: 269–282.

Bellasio C, Beerling DJ, Griffiths H. 2016a. Deriving C_4 photosynthetic parameters from combined gas exchange and chlorophyll fluorescence using an Excel tool: theory and practice. *Plant, Cell & Environment* **39**: 1164–1179.

Bellasio C, Beerling DJ, Griffiths H. 2016b. An Excel tool for deriving key photosynthetic parameters from combined gas exchange and chlorophyll fluorescence: theory and practice. *Plant, Cell & Environment* **39**: 1180–1197.

Bellasio C, Burgess SJ, Griffiths H, Hibberd JM. 2014. A high throughput gas exchange screen for determining rates of photorespiration or regulation of C_4 activity. *Journal of Experimental Botany* **65**: 3769–3779.

Bellasio C, Farquhar GD. 2019. A leaf-level biochemical model simulating the introduction of C_2 and C_4 photosynthesis in C_3 rice: gains, losses and metabolite fluxes. *New Phytologist* **223**: 150–166.

Bellasio C, Griffiths H. 2014a. Acclimation to low light by C_4 maize: implications for bundle sheath leakiness. *Plant, Cell & Environment* **37**: 1046–1058.

Bellasio C, Griffiths H. 2014b. The operation of two decarboxylases (NADPME and PEPCK), transamination and partitioning of C_4 metabolic processes between mesophyll and bundle sheath cells allows light capture to be balanced for the maize C_4 pathway. *Plant Physiology* **164**: 466–480.

Bellasio C, Lundgren MR. 2016. Anatomical constraints to C_4 evolution: light harvesting capacity in the bundle sheath. *New Phytologist* **212**: 485–496.

Bellasio C, Quirk J, Beerling DJ. 2018. Stomatal and non-stomatal limitations in savanna trees and C_4 grasses grown at low, ambient and high atmospheric CO_2. *Plant Science* **274**: 181–192.

Bellasio C, Quirk J, Buckley TN, Beerling D. 2017. A dynamic hydro-mechanical and biochemical model of stomatal conductance for C_4 photosynthesis. *Plant Physiology* **175**: 104–119.

Bellasio C, Quirk J, Ubierna N, Beerling DJ. 2022. Physiological responses to low CO_2 over prolonged drought as primers for forest-grassland transitions. *Nature Plants* **8**: 1014–1023.

Berry JA, Farquhar GD. 1978. The CO_2 concentrating function of C_4 photosynthesis: a biochemical model. In: Hall D, Coombs J, Goodwin T, eds. *Proceedings of the 4th International Congress on photosynthesis, held at the University of Reading, Reading, Berkshire, UK, 4–9 September 1977*. London, UK: The Biochemical Society, 119–131.

Björkman O, Downton WJS, Mooney HA. 1980. Response and adaptation to water stress in Nerium oleander. *Carnegie Institute Washington Yearbook* **79**: 150–157.

Boesgaard KS, Mikkelsen TN, Ro-Poulsen H, Ibrom A. 2013. Reduction of molecular gas diffusion through gaskets in leaf gas exchange cuvettes by leaf-mediated pores. *Plant, Cell & Environment* **36**: 1352–1362.

Buckley TN, Farquhar GD, Mott KA. 1999. Carbon–water balance and patchy stomatal conductance. *Oecologia* **118**: 132–143.

Buckley TN, Mott KA, Farquhar GD. 2003. A hydromechanical and biochemical model of stomatal conductance. *Plant, Cell & Environment* **26**: 1767–1785.

von Caemmerer S. 2000. *Biochemical models of leaf photosynthesis.* Collingwood, Victoria, Australia: CSIRO Publishing.

von Caemmerer S, Evans JR. 1991. Determination of the average partial-pressure of CO_2 in chloroplasts from leaves of several C_3 plants. *Australian Journal of Plant Physiology* **18**: 287–305.

von Caemmerer S, Furbank RT. 1999. Modelling C_4 photosynthesis. In: Sage RF, Monson RK, eds. *The biology of C_4 photosynthesis.* London, UK: Academic Press, 173–211.

Carmo-Silva AE, Soares AS, da Silva JM, da Silva AB, Keys AJ, Arrabaça MC. 2007. Photosynthetic responses of three C_4 grasses of different metabolic subtypes to water deficit. *Functional Plant Biology* **34**: 204–213.

Collatz GJ, Ribas-Carbo M, Berry JA. 1992. Coupled photosynthesis-stomatal conductance model for leaves of C_4 plants. *Australian Journal of Plant Physiology* **19**: 519–538.

Damour G, Simonneau T, Cochard H, Urban L. 2010. An overview of models of stomatal conductance at the leaf level. *Plant, Cell & Environment* **33**: 1419–1438.

Danila FR, Quick WP, White RG, Kelly S, von Caemmerer S, Furbank RT. 2018. Multiple mechanisms for enhanced plasmodesmata density in disparate subtypes of C_4 grasses. *Journal of Experimental Botany* **69**: 1135–1145.

Downton W, Loveys B, Grant W. 1988. Non-uniform stomatal closure induced by water stress causes putative non-stomatal inhibition of photosynthesis. *New Phytologist* **110**: 503–509.

Ethier GJ, Livingston NJ. 2004. On the need to incorporate sensitivity to CO_2 transfer conductance into the Farquhar-von Caemmerer–Berry leaf photosynthesis model. *Plant, Cell & Environment* **27**: 137–153.

Farquhar GD, von Caemmerer S, Berry JA. 1980. A biochemical-model of photosynthetic CO_2 assimilation in leaves of C_3 species. *Planta* **149**: 78–90.

Farquhar GD, Sharkey TD. 1982. Stomatal conductance and photosynthesis. *Annual Review of Plant Physiology and Plant Molecular Biology* **33**: 317–345.

Flexas J, Zhang Y, Gulías J, Xiong D, Carriquí M, Baraza E, Du T, Lei Z, Meng H, Dou H. 2022. Leaf physiological traits of plants from the Qinghai-Tibet Plateau and other arid sites in China: identifying susceptible species and well-adapted extremophiles. *Journal of Plant Physiology* **272**: 153689.

Furbank RT. 2016. Walking the C_4 pathway: past, present, and future. *Journal of Experimental Botany* **67**: 4057–4066.

Ghannoum O. 2009. C_4 photosynthesis and water stress. *Annals of Botany* **103**: 635–644.

Ghannoum O, Conroy JP, Driscoll SP, Paul MJ, Foyer CH, Lawlor DW. 2003. Nonstomatal limitations are responsible for drought-induced photosynthetic inhibition in four C_4 grasses. *New Phytologist* **159**: 599–608.

Ishii R, Yamagishi T, Murata Y. 1977. On a method for measuring photosynthesis and respiration of leaf slices with an oxygen electrode. *Japanese Journal of Crop Science* **46**: 53–57.

Lawlor DW. 2002. Limitation to photosynthesis in water-stressed leaves: stomata vs metabolism and the role of ATP. *Annals of Botany* **89**: 871–885.

Lawlor DW, Cornic G. 2002. Photosynthetic carbon assimilation and associated metabolism in relation to water deficits in higher plants. *Plant, Cell & Environment* **25**: 275–294.

Mott KA, Buckley TN. 1998. Stomatal heterogeneity. *Journal of Experimental Botany* **49**: 407–417.

Nadal M, Flexas J, Gulías J. 2018. Possible link between photosynthesis and leaf modulus of elasticity among vascular plants: a new player in leaf traits relationships? *Ecology Letters* **21**: 1372–1379.

Osborne CP, Sack L. 2012. Evolution of C_4 plants: a new hypothesis for an interaction of CO_2 and water relations mediated by plant hydraulics. *Philosophical Transactions of the Royal Society of London. Series B: Biological Sciences* **367**: 583–600.

Pospíšilová J, Šantrůček J. 1994. Stomatal patchiness. *Biologia Plantarum* **36**: 481–510.

Prioul JL, Chartier P. 1977. Partitioning of transfer and carboxylation components of intracellular resistance to photosynthetic CO_2 fixation: a critical analysis of the methods used. *Annals of Botany* **41**: 789–800.

Quirk J, Bellasio C, Johnson DA, Beerling DJ. 2019a. Response of photosynthesis, growth and water relations of a savannah-adapted tree and grass grown across high to low CO_2. *Annals of Botany* **124**: 77–90.

Quirk J, Bellasio C, Johnson DA, Osborne CP, Beerling DJ. 2019b. C_4 savanna grasses fail to maintain assimilation in drying soil under low CO_2 compared with C_3 trees despite lower leaf water demand. *Functional Ecology* **33**: 388–398.

Rakhmankulova ZF, Shuyskaya EV, Voronin PY, Usmanov IY. 2019. Comparative study on resistance of C_3 and C_4 Xerohalophytes of the genus *Atriplex* to water deficit and salinity. *Russian Journal of Plant Physiology* **66**: 250–258.

Ripley B, Frole K, Gilbert M. 2010. Differences in drought sensitivities and photosynthetic limitations between co-occurring C_3 and C_4 (NADP-ME) Panicoid grasses. *Annals of Botany* **105**: 493–503.

Ripley BS, Gilbert ME, Ibrahim DG, Osborne CP. 2007. Drought constraints on C_4 photosynthesis: stomatal and metabolic limitations in C_3 and C_4 subspecies of *Alloteropsis semialata*. *Journal of Experimental Botany* **58**: 1351–1363.

Rodriguez-Dominguez CM, Buckley TN, Egea G, de Cires A, Hernandez-Santana V, Martorell S, Diaz-Espejo A. 2016. Most stomatal closure in woody species under moderate drought can be explained by stomatal responses to leaf turgor. *Plant, Cell & Environment* **39**: 2014–2026.

Sonawane BV, Koteyeva NK, Johnson DM, Cousins AB. 2021. Differences in leaf anatomy determines temperature response of leaf hydraulic and mesophyll CO_2 conductance in phylogenetically related C_4 and C_3 grass species. *New Phytologist* **230**: 1802–1814.

Takeda T, Fukiyama R. 1981. Effects of mesophyll water potential on photosynthesis in Gramineae plants: with special reference to phylogeny of subfamilies. *Japanese Journal of Crop Science* **50**: 115–116.

Takeda T, Fukiyama R, Ueno O. 1983. Effects of mesophyll water potential on photosynthesis in Cyperaceae plants: with special reference to phylogeny of tribes and decarboxylation sub-types. *Japanese Journal of Crop Science* **52**: 223–224.

Taylor SH, Hulme SP, Rees M, Ripley BS, Ian Woodward F, Osborne CP. 2010. Ecophysiological traits in C_3 and C_4 grasses: a phylogenetically controlled screening experiment. *New Phytologist* **185**: 780–791.

Taylor SH, Ripley BS, Martin T, De-Wet L-A, Woodward FI, Osborne CP. 2014. Physiological advantages of C_4 grasses in the field: a comparative experiment demonstrating the importance of drought. *Global Change Biology* **20**: 1992–2003.

Taylor SH, Ripley BS, Woodward FI, Osborne CP. 2011. Drought limitation of photosynthesis differs between C_3 and C_4 grass species in a comparative experiment. *Plant, Cell & Environment* **34**: 65–75.

Vico G, Porporato A. 2008. Modelling C_3 and C_4 photosynthesis under water-stressed conditions. *Plant and Soil* **313**: 187–203.

Ward JK, Tissue DT, Thomas RB, Strain BR. 1999. Comparative responses of model C_3 and C_4 plants to drought in low and elevated CO_2. *Global Change Biology* **5**: 857–867.

Xu H-l, Ishii R, Yamagishi T, Kumura A. 1990. Effects of water deficit on photosynthesis in wheat plants: III. Effect on non-stomatal mediated photosynthesis and RuBP carboxylase content in different plant parts. *Japanese Journal of Crop Science* **59**: 153–157.

Yang J, Duursma RA, De Kauwe MG, Kumarathunge D, Jiang M, Mahmud K, Gimeno TE, Crous KY, Ellsworth DS, Peters J *et al.* 2019. Incorporating non-stomatal limitation improves the performance of leaf and canopy models at high vapour pressure deficit. *Tree Physiology* **39**: 1961–1974.

Yin X, Struik PC, Romero P, Harbinson J, Evers JB, Van Der Putten PEL, Vos JAN. 2009. Using combined measurements of gas exchange and chlorophyll fluorescence to estimate parameters of a biochemical C_3 photosynthesis model: a critical appraisal and a new integrated approach applied to leaves in a wheat (*Triticum aestivum*) canopy. *Plant, Cell & Environment* **32**: 448–464.

Yin X, Van Oijen M, Schapendonk A. 2004. Extension of a biochemical model for the generalized stoichiometry of electron transport limited C_3 photosynthesis. *Plant, Cell & Environment* **27**: 1211–1222.

Yin XY, Sun ZP, Struik PC, Van der Putten PEL, Van Ieperen W, Harbinson J. 2011. Using a biochemical C_4 photosynthesis model and combined gas exchange and chlorophyll fluorescence measurements to estimate bundle-sheath conductance of maize leaves differing in age and nitrogen content. *Plant, Cell & Environment* **34**: 2183–2199.

Zhou H, Helliker BR, Huber M, Dicks A, Akçay E. 2018. C_4 photosynthesis and climate through the lens of optimality. *Proceedings of the National Academy of Sciences, USA* **115**: 12057–12062.

Supporting Information

Additional Supporting Information may be found online in the Supporting Information section at the end of the article.

Dataset S1 Hydromechanical characterization.

Dataset S2 Photosynthetic responses at full hydration.

Dataset S3 Photosynthetic responses to dehydration.

Fig. S1 Experimental set-up.

Notes S1 Brief description of the mechanistic curve fitting procedures.

Notes S2 Analytical solutions of the model.

Please note: Wiley is not responsible for the content or functionality of any Supporting Information supplied by the authors. Any queries (other than missing material) should be directed to the *New Phytologist* Central Office.